Statistical theory of passive scalar turbulence within the viscous-convective range

Taketo Ariki *
Faculty of Industrial Technology, Tsukuba University of Technology, 4-3-15 Amakubo, Tsukuba 305-8520, Japan

(Received 24 November 2023; accepted 6 May 2024; published 7 June 2024)

An expected statistical law of passive scalar turbulence subjected to high Schmidt numbers is studied with the Hessian-based Lagrangian renormalized approximation (HBLRA), a self-consistent closure theory recently developed for passive scalar turbulence. Without relying on any empirical parameters, HBLRA derives the scalar variance spectrum proportional to k^{-1} in the viscous-convective range predicted by Batchelor. Thanks to improvements in the physical description, HBLRA yields quantitatively better predictions of the scalar variance spectrum and its universal constant in comparison with pioneering closure theories. Our results suggest that the turbulence motion of only a limited scale range may contribute to the scalar flux within the viscous-convective range. Numerical solutions for finite Schmidt numbers (Sc = 10–100 000) are obtained, where a clear viscous-convective range appears with a well-developed inertial-convective range.

DOI: 10.1103/PhysRevFluids.9.064603

I. INTRODUCTION

Fluid turbulence, a class of ubiquitous phenomena in nature, is often characterized by its strong mixing effect, which dominates the transportation of a variety of physical properties, including temperature, chemical substances, etc. A passively convected scalar field is a simplified model of such physical properties, and it offers a basic platform to understand the nature of turbulence mixing.

In the case of sufficiently high Reynolds and Péclet numbers, one may find the inertial-convective range where both fluid dissipation and scalar diffusion are negligible. According to a discussion similar to that of Kolmogorov's inertial range, one may reach the Obukhov-Corrsin scaling law of the scalar structure function [1,2]:

$$\langle[\theta(\mathbf{x}+\mathbf{r})-\theta(\mathbf{x})]^2\rangle \propto \varepsilon^{-1/3}\chi r^{2/3}, \tag{1.1}$$

where θ is the scalar field, $\mathbf{r}$ is a spatial separation within the scale range, and ε and χ are the mean dissipation rate of the kinetic energy and the scalar variance. The scaling law (1.1) may be rewritten in Fourier space; the scalar variance spectrum $E_\theta(k)$ satisfying $\int_0^\infty E_\theta(k)dk = \langle\theta^2\rangle/2$ may be given by a universal power law:

$$E_\theta(k) = C_{OC}\varepsilon^{-1/3}\chi k^{-5/3}, \tag{1.2}$$

where C_{OC} is often referred to as the Obukhov-Corrsin constant. The existence of the power law given by Eq. (1.2) has been suggested from several experiments and direct numerical simulation (DNS) [3–9]. In the inertial-convective range, the above scalar statistics may be understood from a similar mechanism to the Richardson-Kolmogorov cascading of the velocity field: the scalar structure may be destroyed, mostly by turbulence eddies of the same size, and split into smaller pieces.

*ariki@a.tsukuba-tech.ac.jp

While there are a number of phenomena that can be expressed from the mixing taking place in the inertial range, the convection effect of a far smaller lengthscale also plays substantial roles in the real world: clustering of cloud droplets or convection of reactive substances inside water may be typical examples. The fluid convection of such a small lengthscale can be studied using the passive scalar of small diffusivity, which may be characterized by the Schmidt number $\mathrm{Sc} \equiv \nu/\kappa$ (ν is the kinematic viscosity of the fluid, and κ is the diffusivity of the scalar) being sufficiently high, i.e., $S_c \gg 1$. Then one may find in the sub-Kolmogorov scale a subrange called the viscous-convective range where the passive scalar is subjected to persistent straining motions of the Kolmogorov-scale eddies and produces even smaller structures. The problem was first proposed by Batchelor, with his analytical discussions leading to another power law of the scalar-variance spectrum [10]:

$$E_\theta = C_B \chi \left(\frac{\nu}{\varepsilon}\right)^{1/2} k^{-1} \quad (k_\eta \ll k \ll k_b), \tag{1.3}$$

where C_B, often referred to as the Batchelor constant, is expected as another universal constant, $k_\eta (\equiv 1/\eta)$, is the Kolmogorov wave number defined as the reciprocal of the Kolmogorov length $\eta\,[\equiv(\nu^3/\varepsilon)^{1/4}]$, and $k_b (\equiv 1/\eta_b)$ is the Batchelor wave number defined as the reciprocal of the Batchelor length $\eta_b\,[\equiv(\kappa^2\nu/\varepsilon)^{1/4}]$. The above spectrum can also be derived from the dimensional analysis using Kolmogorov's timescale $(\nu/\varepsilon)^{1/2}$, and the turbulence mixing in the viscous-convective range may be dominated by the motion of the smallest turbulence eddies at the Kolmogorov scale. Then, unlike the scale-local mechanism of the Richardson-Kolmogorov cascading, turbulence mixing in the sub-Kolmogorov range may be understood from the scale nonlocal interaction between the Kolmogorov and sub-Kolmogorov scales, which has quite a different mechanism from those in the inertial range, and it has yet to be explored.

Since the discovery by Ref. [10], considerable efforts have been devoted to investigating the nature of the viscous-convective range from experimental [11–13], numerical [6,14–17], and theoretical frameworks [18,19]. Among them, experiment and DNS, which are direct approaches to the problem, may still have severe limitations in either Reynolds or Schmidt numbers, since the situation requires a huge gap between the largest and the smallest scales. Thus, in this paper we choose one of the theoretical approaches, namely self-consistent spectral closure. Since the early work of the direct-interaction approximation (DIA) [20], self-consistent spectral closure has offered deductive approaches to the lower-order statistics of turbulence on the basis of the exact governing law. The Lagrangian-history DIA (LHDIA) [21] may be the pioneering attempt to incorporate the Lagrangian picture into DIA strategy, resulting in self-consistent closure models consistent with Kolmogorov's theory, e.g., abridged Lagrangian history DIA (ALHDIA) [21] and strain-based ALHDIA (SBALHDIA) [22]. On the other hand, Kraichnan presented a more systematic scheme to obtain his closure models on the basis of what is called the renormalized-perturbation theory [23]. Here we should mention the Lagrangian description of the field, a fundamental building block of the Lagrangian closure families. In the Lagrangian description, one may focus on the dynamics of the field value experienced by a fluid element, and the fluid element may be identified by a space-time point, say $(\mathbf{x}, s)$, passed by the trajectory of the element. Then a field value ϕ experienced at time t by an element labeled by $(\mathbf{x}, s)$ may be written as $\phi(\mathbf{x}, s|t)$. The original idea of the Lagrangian picture is to focus on the time advancement in t which is referred to as the *measuring time* in Ref. [24]. However, in LHDIA-based theories, the true Lagrangian dynamics of variables are avoided due to their mathematical complexity, and instead s, referred to as the *labeling time* in Ref. [24], is chosen for the development of the two-time statistics. This point was substantially improved by Kaneda [24]: the Lagrangian position function, a mapping function from the Eulerian to Lagrangian variables, was introduced for a more direct treatment of the Lagrangian time advancement of variables. The resultant theory—the Lagrangian renormalized approximation (LRA)—enables far simpler closure equations. In particular, the fluctuation-dissipation relation [Eq. (2.53) of Ref. [24]] reduces its calculation cost appreciably, although it is not yet known whether this is a natural consequence or just an accident. Later, the LRA model was rederived on the basis of the DIA formalism instead of the renormalization scheme [25]. While not fully

justified because of their deficiency in describing higher-order statistics, self-consistent spectral closures enable us to investigate large-scale phenomena of very high Reynolds and Schmidt numbers far out of reach of both DNS and experiments of current technologies. There was, however, a specific problem involving self-consistent closure when applied to passive scalar turbulence: while successful at the level of dimensional analysis, these closure theories underestimate the scalar variance spectrum in general [26–30]. A recent work on self-consistent spectral closure focused on this problem and proposed an improved version of LRA, namely the Hessian-based LRA (HBLRA) [31]. Thanks to its theoretical basis on the local scalar structure, HBLRA succeeded, without relying on any empirical parameters, in deriving the inertial-convective spectrum with the Obukhov-Corrsin constant being $C_{OC} \approx 0.754$, which is reasonably close to experimental and DNS data of $C_{OC} \approx 0.7$ [5–9]. In addition to passive scalar statistics, HBLRA has also been applied to the inertial particle problem to elucidate the interscale dynamics of particle clusters [32].

This paper provides theoretical analyses of the passive scalar statistics of high Schmidt numbers on the basis of HBLRA, whose short introduction is given in the forthcoming Sec. II. The closed set of equations provided by HBLRA enables a self-consistent description of the scalar variance spectrum coupled with background turbulence. In Sec. III, an asymptotic analysis is applied to HBLRA to obtain a closed set of equations for the far-dissipative range describing the nonlocal coupling between turbulence and scalar. In Sec. IV, without relying on any empirical parameters, Batchelor's spectrum [Eq. (1.3)] and its universal constant are derived from the asymptotic solution of the high-Schmidt-number limit. Finite-Schmidt-number cases are also investigated in Sec. V, where we see in a quantitative manner how the viscous-convective range develops as the Schmidt number increases.

II. SUMMARY OF HBLRA

Here we provide a brief summary of HBLRA theory (see Ref. [31] for more details). HBLRA is a branch of Lagrangian renormalized approximation (LRA) theory [24]. The essential difference of HBLRA from conventional theories is its closure variable representing the scalar statistics. In the renormalized perturbation theory in turbulence, the choice of the representative variable is the key to a better approximation [24,33].

In contrast to the pioneering works employing the scalar field $\theta(\mathbf{x}, t)$ itself, we shall focus on an alternative quantity representing more structural information of the local scalar distribution, which may be the key idea of Batchelor's theory [10]. The scalar Hessian, $\partial_i \partial_j \theta$, may be the most fundamental quantity expressing local extrema and saddle points of scalar distribution. However, the Hessian, the second-order derivative of the scalar, is too sensitive to the small-scale nature, so we focus instead on a spatially integrated Hessian $\bar{\mathscr{H}}_{ij} \equiv \triangle^{-1} \partial_i \partial_j \theta$. One thing to note is that $\bar{\mathscr{H}}$ reflects the value of the scalar gradient, unlike the pure Hessian $\partial_i \partial_j \theta$, which may be understood from $\partial_i \bar{\mathscr{H}}_{ij} = \partial_j \theta$. Thus the local value of $\bar{\mathscr{H}}_{ij}$ may also be sensitive to the large-scale structure acting like a background scalar gradient, which may be an undesirable feature as a closure variable expressing small-scale nature. Then the following quantity is chosen as the representative variable of HBLRA:

$$\mathscr{H}_{ij} \equiv \bar{\mathscr{H}}_{ij} - \delta_{ij}\theta. \tag{2.1}$$

Here the term $-\delta_{ij}\theta$ is added to cancel out the dependence on the scalar gradient (see discussions in Sec. II B of Ref. [31]). Following the original LRA, we apply the Lagrangian analysis to the modified Hessian $\mathscr{H}_{ij}$, which describes the deformation of the local scalar distribution in the Lagrangian picture.

For later discussions, we assume homogeneity and isotropy of both the velocity and the scalar fields. Thereby, the Fourier analysis in the spatial components may be available in describing the dynamics of each scale. We define the Fourier transformation as follows:

$$\mathscr{H}_{ij}(\mathbf{x}, t) \to \mathscr{H}_{ij}(\mathbf{k}, t) = \frac{1}{(2\pi)^3} \int d^3x \exp\left[-i\mathbf{k} \cdot \mathbf{x}\right] \mathscr{H}_{ij}(\mathbf{x}, t), \tag{2.2}$$

where the Fourier component $\mathscr{H}_{ij}(\mathbf{k},t)$ shares the same main symbol with the spatial component $\mathscr{H}_{ij}(\mathbf{x},t)$ for simplicity of notation. Following similar steps to the original LRA theory, the autocorrelation and the averaged response function of the Hessian $\mathscr{H}_{ij}$ are introduced. In the homogeneous and isotropic cases, all the statistical functions may be reduced to isotropic scalar functions: $Q(k;t,t')$, $H(k;t,t')$, and $G_H(k;t,t')$ for the velocity autocorrelation, the Hessian autocorrelation, and the Hessian response function, respectively ($k \equiv \|\mathbf{k}\|$). The scalar variance spectrum $E_\theta(k)$ is related to our Hessian autocorrelation by $E_\theta(k,t) = 4\pi k^2 H(k;t,t)$, so it is solved from the closure equations for $Q(k;t,t')$, $H(k;t,t')$, and $G_H(k;t,t')$. If the scalar source is confined in a sufficiently small wave number region, HBLRA theory yields the following set of equations for $H(k;t,t')$ and $G_H(k;t,t')$:

$$(\partial_t + 2\kappa k^2)H(k;t,t) = 2\pi \iint_\triangle dp\,dq\,kpq(1-z^2)\int_{t_0}^{t} ds Q(p;t,s) \times \{H(q;s,t)G_H(k;t,s) - H(k;s,t)G_H(q;t,s)\}, \tag{2.3}$$

$$(\partial_t + \kappa k^2)H(k;t,t') = -\frac{\pi}{2}\iint_\triangle dp\,dq\,kpq(1-y^2)(1-z^2)\int_{t'}^{t} ds\, Q(p;t,s)H(k;t,t') - \frac{\pi}{2}\iint_\triangle dp\,dq\,kpq(1-y^2)(1-z^2)\int_{t_0}^{t} ds\, Q(p;t,s)G_H(q;t,s)H(k;s,t') + \frac{\pi}{2}\iint_\triangle dp\,dq\,kpq(1-y^2)(1-z^2)\int_{t_0}^{t'} ds\, Q(p;t,s)H(q;t,s)G_H(k;t',s), \tag{2.4}$$

$$(\partial_t + \kappa k^2)G_H(k;t,t') = -\frac{\pi}{2}\iint_\triangle dp\,dq\,kpq(1-y^2)(1-z^2) \times \int_{t'}^{t} ds\, Q(p;t,s)\{G_H(k;t,t') + G_H(q;t,s)G_H(k;s,t')\} \quad (t \geqslant t'), \tag{2.5}$$

$$G_H(k;t',t') = 1, \tag{2.6}$$

while the velocity autocorrelation $Q(k;t,t')$ is obtained from the LRA equations for the velocity closure [Eqs. (2.35)–(2.46) of Ref. [24]] and is related to the energy spectrum $E(k,t)$ as $E(k,t) = 2\pi k^2 Q(k;t,t)$. The geometrical factors $y \equiv (q^2+k^2-p^2)/(2kq)$, $z \equiv (p^2+k^2-q^2)/(2kp)$, and $\triangle \equiv \{(p,q)|\ |k-p| \leqslant q \leqslant k+p\}$ reflect the triad interaction between three wave number modes: second-order nonlinearity allows for an interaction between three modes when k, p, and q can form the sides of a triangle. Then three factors x [$\equiv(p^2+q^2-k^2)/(2pq)$], y, and z are introduced as cosines of three interior angles opposite to the sides k, p, and q, respectively [20,24]. The integration domain $\triangle$ arises from an existence condition for such a triangle.

III. EQUATIONS FOR THE FAR-DISSIPATIVE RANGE

If turbulence is sustained by a source applied in a sufficiently large scale, the inertial range may span a wide range in Fourier space. Let $Q(k;t,t)$ be $C_K\varepsilon^{2/3}k^{-11/3}$ for $k \to +0$ so that the inertial range reaches the neighbor of $k=0$, which corresponds to the high-Reynolds-number limit. $Q(k)$ can be solved under such a condition, and the resultant 3D energy spectrum $E(k) \equiv 2\pi k^2 Q(k;t,t)$ is given in Fig. 1. The Kolmogorov constant was obtained as $C_K \approx 1.722$ in a similar manner to

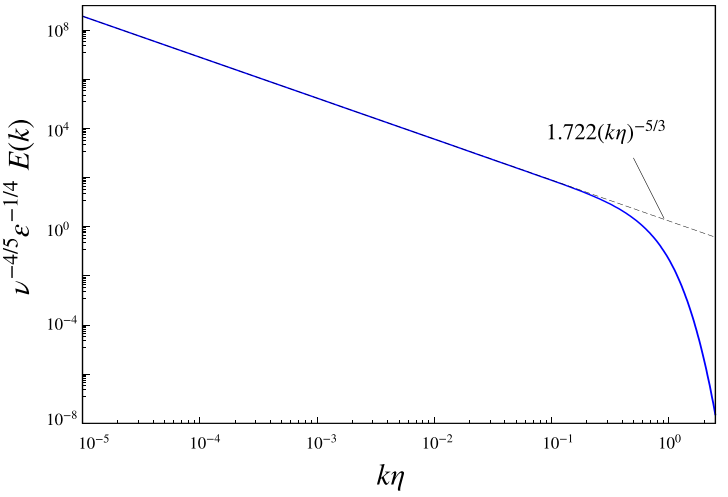

FIG. 1. Energy spectrum function $E(k) \equiv 2\pi k^2 Q(k;t,t)$ obtained from LRA. A numerical factor 1.722 corresponds to the Kolmogorov constant C_K.

that of Ref. [28]. Note that the value agrees with that of Ref. [25] ($C_K \approx 1.722$) based on a different calculation scheme from those of the present work and Ref. [28]. At a sufficiently high wave number $k \gg k_\eta$, where the viscosity sufficiently suppresses the energy spectrum, HBLRA closure composed of Eqs. (2.3)–(2.6) is reduced to a much simpler form. First, let k be sufficiently higher than k_η. Then $Q(p;t,s)$ in Eqs. (2.3)–(2.5) vanishes in most of the integration domain $\triangle$ except for the region $p \ll k$. Let us introduce here a cutoff wave number $p_{\max}$ satisfying $k_\eta \ll p_{\max} \ll k$. Then, only a limited part $\triangledown \equiv \{(p,q)|\ |k-p| \leqslant p \leqslant p_{\max}\}$ in the total integration domain $\triangle$ may be sufficient to reach appropriate values of the nonlinear terms (see Fig. 2). The resultant equations read

$$\left(\partial_t + 2\kappa k^2\right) H(k;t,t) = \frac{4}{15}\pi k^{-2} \int_0^\infty dp \int_{t_0}^t ds\ p^4 Q(p;t,s) \times \left[G_H(k;t,s) \frac{\partial}{\partial k} \left\{ k^4 \frac{\partial H(k;s,t)}{\partial k} \right\} - H(k;s,t) \frac{\partial}{\partial k} \left\{ k^4 \frac{\partial G_H(k;t,s)}{\partial k} \right\} \right], \tag{3.1}$$

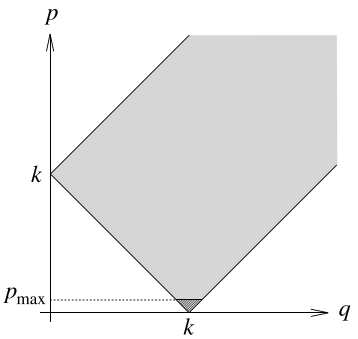

FIG. 2. In the case of $k \gg p$, most of the velocity correlation $Q(p;t,s)$ is confined in the range $0 \leqslant p \leqslant p_{\max}$, so that the integration domain can be reduced from $\triangle$ (gray area) to $\triangledown$ (hatched area) in calculating the nonlinear terms of Eqs. (2.3)–(2.5).

$$(\partial_t + \kappa k^2)H(k;t,t') = -\frac{8}{15}\pi \int_0^\infty dp \int_{t'}^t ds\, p^4 Q(p;t,s)H(k;t,t') - \frac{8}{15}\pi \int_0^\infty dp \int_{t_0}^t ds\, p^4 Q(p;t,s)G_H(k;t,s)H(k;s,t') + \frac{8}{15}\pi \int_0^\infty dp \int_{t_0}^{t'} ds\, p^4 Q(p;t,s)H(k;t,s)G_H(k;t',s), \tag{3.2}$$

$$(\partial_t + \kappa k^2)G_H(k;t,t') = -\frac{8}{15}\pi \int_0^\infty dp \int_{t'}^t ds\, p^4 Q(p;t,s) \times \{G_H(k;t,t') + G_H(k;t,s)G_H(k;s,t')\} \quad (t \geqslant t'), \tag{3.3}$$

whose derivation may be given in Appendix A. Now Eqs. (3.1)–(3.3) accompanied by $G_H(k;t',t') = 1$ [see Eq. (2.6)] form a closed set of equations for the scalar statistics at the far-dissipative scale $k \gg k_\eta$. Unlike the original Eqs. (2.3)–(2.5), the wave number integration is applied only on the velocity correlation, which implies that the self-interaction of the scalar is now quite local while the coupling between the scalar and the velocity is nonlocal. Recalling that $E(p) = 2\pi p^2 Q(p)$, we notice that $p^4 Q(p;t,s)$ in Eqs. (3.1)–(3.3) is closely related to the autocorrelation of the velocity strain, which becomes prominent around the Kolmogorov scale. Then the timescale of the local scalar structure may be mostly dominated by the balance between the timescale of the straining motion around the Kolmogorov scale and the diffusion timescale.

IV. VISCOUS-CONVECTIVE RANGE

In the case of high Schmidt numbers, we may find within the viscous range a subrange where the convection effect exceeds the scalar diffusion. In such a scale range, diffusion terms in Eqs. (3.1)–(3.3) may be negligible. Then we soon realize that Eq. (3.3) without the diffusion term can be uniquely solved without a dependence on k. Let us normalize Eq. (3.3) by the Kolmogorov scales of length and time. We introduce a dimensionless time interval as $\tau \equiv (t-t')(\varepsilon/\nu)^{1/2}$. Now we rewrite G_H as follows using a dimensionless function $\bar{G}_H$:

$$G_H(k;t,t') = \bar{G}_H(\tau). \tag{4.1}$$

In a similar fashion, the velocity correlation $Q(p;t,s)$ can also be rewritten using another dimensionless function $\bar{Q}$:

$$Q(p;t,s) = \frac{C_K}{2\pi}\varepsilon^{2/3}p^{-11/3}\bar{Q}(\bar{p};\tau-\sigma), \tag{4.2}$$

where $\bar{p} \equiv p\eta$ is a dimensionless wave number, $\sigma \equiv (s-t')(\varepsilon/\nu)^{1/2}$ is another dimensionless time, and C_K ($\approx$1.722 [25,28]) is the Kolmogorov constant. Then Eq. (3.3) may be rewritten as

$$\partial_\tau \bar{G}_H(\tau) = -\frac{4}{15}C_K \int_0^\infty d\bar{p}\, \bar{p}^{1/3} \int_0^\tau d\sigma\, \bar{Q}(\bar{p};\tau-\sigma)\{\bar{G}_H(\tau) + \bar{G}_H(\tau-\sigma)\bar{G}_H(\sigma)\} \quad (\tau \geqslant 0). \tag{4.3}$$

Now $\bar{G}_H(\tau)$ can be uniquely solved using $\bar{G}_H(0) = 1$. The numerical result of $\bar{G}_H(\tau)$ is given in Fig. 3. Some details of the calculus to solve Eq. (4.3) can be found in Appendix B. Now the response function $G_H(k;t,t')$ tells us the relaxation of the local scalar structure, whose time integration offers the timescale of the scalar field:

$$\tau_G \equiv \int_t^\infty G_H(k;t',t)dt' = (\nu/\varepsilon)^{1/2}\int_0^\infty \bar{G}_H(\tau)d\tau \approx 2.53(\nu/\varepsilon)^{1/2} \tag{4.4}$$

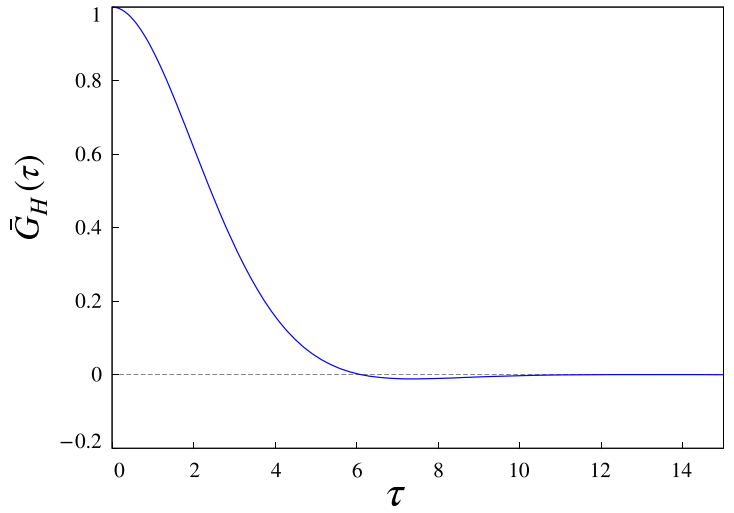

FIG. 3. Numerical result of $\bar{G}_H$. The dimensionless time interval τ (horizontal axis) is normalized by the Kolmogorov timescale $(\nu/\varepsilon)^{1/2}$.

in the unit of the Kolmogorov timescale $(\nu/\varepsilon)^{1/2}$. It should be remarked that the scalar structures in the viscous-convective range have a single timescale τ_G independent of k, which agrees with the idea of Ref. [10]: the scalar structures within the viscous-convective range are uniformly deformed by the turbulence eddy of the Kolmogorov length, and they have a single timescale $(\nu/\varepsilon)^{1/2}$. A similar approach may be applicable to Eq. (3.2). Here we focus on another correlation function instead of $H(k;t,t')$. If the scalar field reaches the stationary state, we can introduce a normalized function:

$$R_H(k;t,t') \equiv \frac{H(k;t,t')}{H(k;t,t)}, \tag{4.5}$$

whose equation may be given by

$$\begin{aligned}\partial_t R_H(k;t,t') = &-\frac{8}{15}\pi\int_0^\infty dp\int_{t'}^t ds\, p^4 Q(p;t,s)R_H(k;t,t') - \frac{8}{15}\pi\int_0^\infty dp\int_{t_0}^t ds\, p^4 Q(p;t,s)\\ &\times G_H(k;t,s)R_H(k;s,t') + \frac{8}{15}\pi\int_0^\infty dp\int_{t_0}^{t'} ds\, p^4 Q(p;t,s)R_H(k;t,s)G_H(k;t',s),\end{aligned} \tag{4.6}$$

accompanied by $R_H(k;t',t') = 1$. Due to the independence of G_H from k, Eq. (4.6) can be uniquely solved without a dependence on k. Using another dimensionless function $\bar{R}_H$, we rewrite R_H in a dimensionless form:

$$R_H(k;t,t') = \bar{R}_H(\tau), \tag{4.7}$$

where τ is again the dimensionless time $(t-t')(\varepsilon/\nu)^{1/2}$. By introducing again the dimensionless wave number $\bar{p} \equiv p\eta$, Eq. (4.6) may be rewritten as

$$\begin{aligned}\partial_\tau \bar{R}_H(\tau) = &-\frac{4}{15}C_K\int_0^\infty d\bar{p}\,\bar{p}^{1/3}\int_0^\tau d\sigma\,\bar{Q}(\bar{p};\sigma)\bar{R}_H(\tau) - \frac{4}{15}C_K\int_0^\infty d\bar{p}\,\bar{p}^{1/3}\int_{-\infty}^\tau d\sigma\,\bar{Q}(\bar{p};\tau-\sigma)\\ &\times\bar{G}_H(\tau-\sigma)\bar{R}_H(\sigma) + \frac{4}{15}C_K\int_0^\infty d\bar{p}\,\bar{p}^{1/3}\int_{-\infty}^0 d\sigma\,\bar{Q}(\bar{p};\tau-\sigma)\bar{R}_H(\tau-\sigma)\bar{G}_H(-\sigma),\end{aligned} \tag{4.8}$$

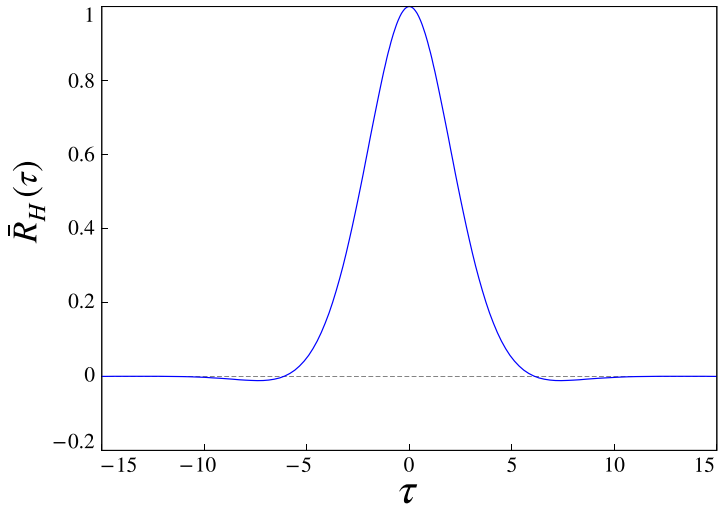

FIG. 4. Numerical result of $\bar{R}_H$.

accompanied by $\bar{R}_H(0) = 1$. The numerical solution of $\bar{R}_H(\tau)$ is given in Fig. 4, which is symmetric under a transformation $\tau \to -\tau$, i.e., $H(k;t,t') = H(k;t',t)$ holds in the viscous-convective range. The timescale is given by

$$\tau_R \equiv \frac{1}{2}\int_{-\infty}^{\infty} R_H(k;t',t)dt' = \frac{1}{2}(\nu/\varepsilon)^{1/2}\int_{-\infty}^{\infty}\bar{R}_H(\tau)d\tau \approx 2.53(\nu/\varepsilon)^{1/2}, \tag{4.9}$$

which coincides exactly with τ_G.

Now we are ready to solve the scalar spectrum using Eq. (3.1). Multiplying both sides of Eq. (3.1) by $4\pi k^2$, we obtain the equation of the scalar variance spectrum:

$$(\partial_t + 2\kappa k^2)E_\theta(k,t) = T_\theta(k,t), \tag{4.10}$$

where T_θ is the transfer function of the scalar variance spectrum:

$$T_\theta(k,t) = \frac{16}{15}\pi^2\int_0^\infty dp\int_{t_0}^t ds\, p^4 Q(p;t,s) \times\left[G_H(k;t,s)\frac{\partial}{\partial k}\left\{k^4\frac{\partial H(k;s,t)}{\partial k}\right\} - H(k;s,t)\frac{\partial}{\partial k}\left\{k^4\frac{\partial G_H(k;t,s)}{\partial k}\right\}\right]. \tag{4.11}$$

Under the stationary state, the time-derivative term on the left side of Eq. (4.10) vanishes. Also, the diffusion term vanishes in the viscous-convective range. Then, integrating Eq. (4.10) over $[k,\infty)$ yields

$$\int_k^\infty T_\theta(p)dp = 2\kappa\int_k^\infty p^2 E_\theta(p)dp = \chi, \tag{4.12}$$

i.e., the scalar flux $\Pi_\theta(k) \equiv \int_k^\infty T_\theta(p)dp$ may take a constant value χ in the viscous-convective range. Recalling that both G_H and R_H are independent of k in the viscous-convective range (see Sec. IV), Eq. (4.11) may be rewritten as

$$T_\theta(k) = \frac{16}{15}\pi^2\frac{\partial}{\partial k}\left[k^4\frac{\partial H(k)}{\partial k}\right]\int_0^\infty dp\int_{t_0}^t ds\, p^4 Q(p;t,s)R_H(k;s,t)G_H(k;t,s), \tag{4.13}$$

while the scalar-variance flux $\Pi_\theta(k)$ is given by

$$\Pi_\theta(k) = -\frac{16}{15}\pi^2 k^4 \frac{\partial H(k)}{\partial k} \int_0^\infty dp \int_{-\infty}^t ds\; p^4 Q(p;t,s) R_H(k;s,t) G_H(k;t,s). \tag{4.14}$$

With the help of Eq. (4.14), Eq. (4.12) can be rewritten as a first-order differential equation of $E_\theta(k)$ (see Appendix C), whose solution may be given by

$$E_\theta(k) = C_B \chi \left(\frac{\nu}{\varepsilon}\right)^{1/2} k^{-1}, \tag{4.15}$$

where

$$C_B = \frac{5}{2C_K} \Big/ \int_0^\infty d\bar{p}\; \bar{p}^{1/3} \int_0^\infty d\sigma\; \bar{Q}(\bar{p},\sigma) \bar{R}_H(-\sigma) \bar{G}_H(\sigma). \tag{4.16}$$

Now Eq. (4.15) is identical to the expected Batchelor spectrum of Eq. (1.3). Then C_B given by Eq. (4.16) is identified with the Batchelor constant. Numerical calculation of Eq. (4.16) yields

$$C_B \approx 3.60, \tag{4.17}$$

which is close to the experimental values obtained from the measurements of oceanic flows (3.9 ± 1.5 [11] and 3.7 ± 1.5 [12]). The present achievement (4.17) should be compared with the results from the pioneering Lagrangian-closure theories: $\sqrt{10/3}(\approx 1.83)$ from LRA [34], 1.30 from LDIA (its fundamental equations are identical to those of LRA) [29], 0.8–1.0 from ALHDIA [27], and 2.0 from SBALHDIA [27], which are all substantially lower than the present result. The discrepancy between the present and the pioneering results comes exactly from the difference in their physical pictures: in the present theory, the two-time statistics $G_H(k;t,s)$ and $H(k;t,s)$ explain the timescale of the deformation of the scalar distribution caused by fluid's straining motion, and they express the scalar flux within the viscous-convective range according to Eq. (4.14). In contrast, the pioneering theories are incapable of describing the timescale of the scalar deformation because of their representative variables being the scalar field, and the deformation of the scalar is irrelevant to determine the scalar flux within the viscous-convective range, which may be inconsistent with the idea of Batchelor [10]. This may be understood from the behavior of the scalar value experienced by a Lagrangian fluid element: if the diffusivity is sufficiently small, the scalar value on a fluid element may be conserved, yielding an infinite-length timescale in its Lagrangian analysis. This amounts to a simple replacement $G_H(k;t,t')$, $R_H(k;t,t') \to 1$ of Eq. (4.14). As a result, the conventional Lagrangian theories based on the scalar field explain their scalar flux without the relaxation effect of the deformation of the scalar field, and they overestimate the scalar flux and underestimate C_B.

Now Eq. (4.14) expresses the scalar-variance flux by integrating the contributions from the velocity-gradient statistics of various scales. One can discuss the weight of the contribution from the velocity gradient of each scale. Let us rewrite Eq. (4.14) as

$$\Pi_\theta(k) = -\frac{2}{15} C_K \left(\frac{\varepsilon}{\nu}\right)^{1/2} k^3 \frac{\partial\, k^{-1} E_\theta(k)}{\partial k} \int_0^\infty d\bar{p}\, W(\bar{p}), \tag{4.18}$$

where $W(\bar{p})$ is a dimensionless function given by

$$W(\bar{p}) = \int_0^\infty d\sigma\; \bar{p}^{1/3} \bar{Q}(\bar{p},\sigma) \bar{R}_H(-\sigma) \bar{G}_H(\sigma).$$

Another dimensionless function

$$\bar{W}(\bar{p}) \equiv \frac{W(\bar{p})}{\int_0^\infty d\bar{q}\, W(\bar{q})} \tag{4.19}$$

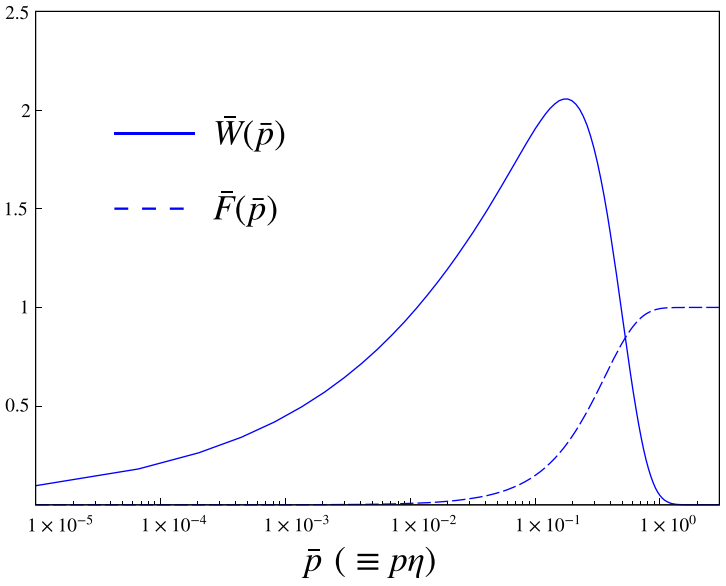

FIG. 5. Dimensionless measures $\bar{W}$ and $\bar{F}$ of the contribution from the velocity gradient to the scalar flux. In the horizontal axis, the wave number $\bar{p}$ is normalized by the Kolmogorov length η.

offers a measure of the contribution from the velocity gradient statistics at the scale of $\bar{p}$. An integral of $\bar{W}$, i.e.,

$$\bar{F}(\bar{p}) \equiv \int_0^{\bar{p}} \bar{W}(\bar{q}) d\bar{q}, \tag{4.20}$$

tells us how much the scalar flux is generated by the fluid motion at the wave number range lower than $\bar{p}$. Numerical results of the measures $\bar{W}$ and $\bar{F}$ are plotted in Fig. 5. $\bar{W}$ increases monotonically before its peak around $\bar{p} = 0.1$. Recalling that $\bar{p}$ is normalized by the Kolmogorov length η, $\bar{p} = 0.1$ corresponds to $0.1k_\eta$ in the wave number, which is close to the scale at which the dissipation spectrum peaks. This suggests that the dissipative motion of the fluid gives a major contribution to the scalar flux in the viscous-convective range. In contrast, $\bar{F}(\bar{p})$ remains 0.15 at $\bar{p} = 0.1$, meaning that only 15% of the scalar flux within the viscous-convective range is induced by the fluid motion of the wave number range smaller than $0.1k_\eta$. On the other hand, $\bar{F}(\bar{p})$ reaches 0.99 at $\bar{p} = 0.9$, suggesting that the fluid motion of $k \geqslant 0.9k_\eta$ contributes only 1%. Also, one may say that more than 80% (99–15%) of the scalar flux can be expressed by the fluid motion within the wave number band $[0.1k_\eta, 0.9k_\eta]$. In addition, $\bar{F}(1) \approx 0.995$ and $\bar{F}(0.01) \approx 0.005$, so the fluid motion within $[0.01k_\eta, k_\eta]$ can express 99% (99.5–0.5%) of the scalar flux within the viscous-convective range.

V. SOLUTIONS FOR FINITE SCHMIDT NUMBERS

So far we have applied an asymptotic analysis to HBLRA equations in order to investigate the physics of the high-Schmidt-number limit, which could hardly be achieved by experiment nor DNS in the near future. On the other hand, the case of finite Schmidt numbers can be solved from HBLRA equations in a straightforward manner, which may offer some cornerstones for near-future studies. In the present work, stationary solutions of finite Schmidt numbers varying from 10 to 100 000 are obtained, with a slight modification to HBLRA equations for the sake of reducing the calculation cost; since most of the calculation cost of HBLRA is from the triple integrals on the right side

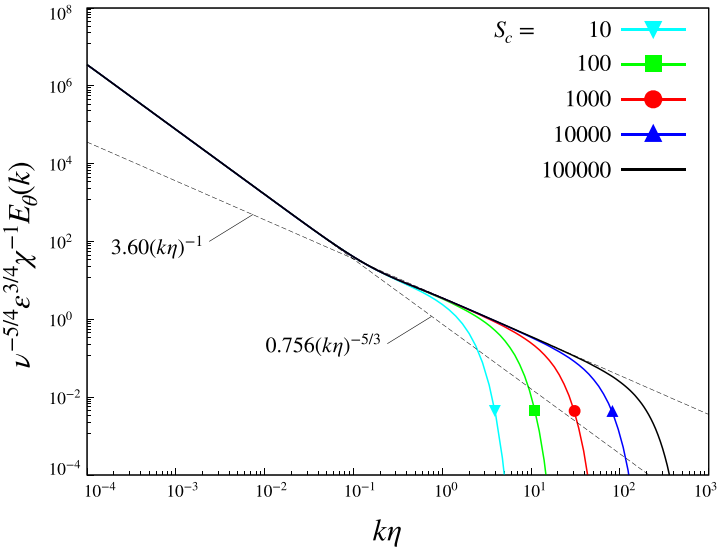

FIG. 6. Scalar variance spectra. Dotted lines show the theoretical asymptotes of the inertial-convective and the viscous-convective ranges, respectively.

of Eq. (2.4), we redefine $H(k;t',t)$ as $H(k;t,t')$ for $t \geqslant t'$. As mentioned in the previous section, $H(k;t,t') = H(k;t',t)$ holds in the viscous-convective range, so the current modification does not alter the result of the viscous-convective solution, while a slight difference appears in the inertial-convective range: the Obukhov-Corrsin constant becomes $C_{OC} \approx 0.756$, which is almost identical to the original result $C_{OC} \approx 0.754$.

Here we employ the same velocity statistics $Q(k;t,t')$ in the previous sections. Provided the scalar field is sustained by its source of sufficiently large scale, we apply $H(k) = (4\pi)^{-1} C_{OC} \chi \varepsilon^{-1/3} k^{-11/3}$ for $k \to 0$ as a boundary condition to solve Eqs. (2.3)–(2.6). The resultant spectra are shown in Fig. 6, where the power law region $\propto k^{-1}$ observed in $k\eta \gtrsim 0.1$ extends as the Schmidt number increases. To see more details of the viscous-convective range, the compensated spectra are shown in Fig. 7. A buffer region $0.05 \lesssim k\eta \lesssim 1$ may be recognized between the inertial-convective and the viscous-convective ranges, and the k^{-1} range may exist in $k\eta \gtrsim 1$. Then $S_c = 10$ and 100 may not be sufficient to observe the asymptote of $C_B \approx 3.60$ beyond the buffer. In the inset of Fig. 7, we draw an error band of 3% (a green band) ranging from 3.49 to 3.71 of the vertical axis in order to identify the plateaus such that the compensated spectra agree with $C_B \approx 3.60$ within an error of 3%. Then $0.8 \lesssim k\eta \lesssim 10$ from the case of Sc = 10 000 and $0.8 \lesssim k\eta \lesssim 30$ from the case of Sc = 100 000 are identified. In addition to the scalar variance spectrum of the single-time analysis, HBLRA expresses the timescale of the scalar field from the two-time statistics, i.e., $\tau_G \equiv \int_t^\infty G_H(k;t',t)dt'$ [see also Eq. (4.4)] plotted in Fig. 8. Again, a buffer region $0.05 \lesssim k\eta \lesssim 1$ appears between the inertial-convective and the viscous-convective ranges. In the viscous-convective range above the buffer region, the timescale τ_G tends to a constant, which indicates that the scalar timescale within the viscous-convective range is uniformly dominated by a single timescale $(\nu/\varepsilon)^{1/2}$. Again, the error band of 3% ranging from 2.45 to 2.61 of the vertical axis is drawn in the inset of Fig. 8 (a green band). Then the plateaus $1 \lesssim k\eta \lesssim 10$ from the case of Sc = 10 000 and $1 \lesssim k\eta \lesssim 50$ from the case of Sc = 100 000 are identified, respectively. For both the spectrum and the timescale, the plateaus may extend as Sc increases.

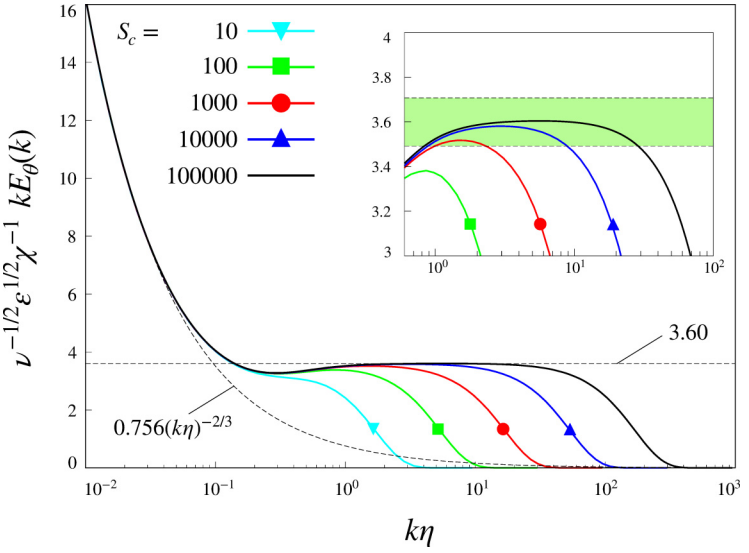

FIG. 7. Compensated spectra. Dotted lines show the theoretical asymptotes of the inertial-convective and the viscous-convective ranges, respectively.

VI. SUMMARY AND DISCUSSIONS

Passive scalar turbulence at high Schmidt numbers was examined by means of HBLRA, a self-consistent closure theory based on the exact governing laws. Without relying on any empirical parameters, the closure equations successfully led us to an expected result $\propto k^{-1}$ of the scalar variance spectrum within the viscous-convective range with its universal Batchelor constant $C_B \approx 3.60$ [see Eq. (4.17)], which is appreciably larger than those obtained from pioneering closure

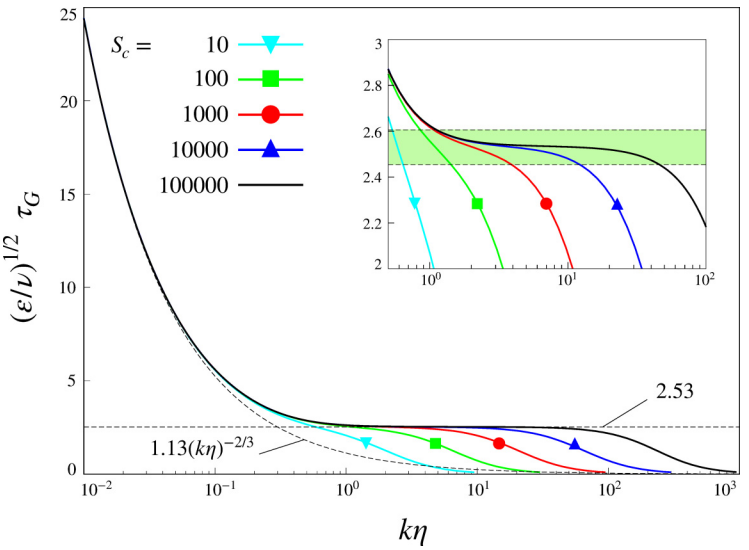

FIG. 8. Scalar timescale τ_G. Dotted lines show the theoretical asymptotes of the inertial-convective and the viscous-convective ranges, respectively. The timescale of the inertial-convective range is obtained as $1.13k^{-2/3}\varepsilon^{-1/3}$ in Ref. [31].

theories: LRA (1.30–1.83), ALHDIA (0.8–1.0), and SBALHDIA (2.0). Experiments and DNS suggest $C_B \approx 3.6$–5.7, thus, at least in terms of the predictability of the Batchelor constant, HBLRA may be the most reliable among these self-consistent closure theories (there is also an estimation $C_B = 2\sqrt{5} \approx 4.47$ based on the Langevin models of the velocity and the scalar within the Eulerian framework [19]). This may be because of the improvement in the physical picture: unlike pioneering theories, HBLRA successfully explained the timescale of a scalar within the viscous-convective range deformed by the straining motion of the Kolmogorov scale, which leads to a more plausible description of the viscous-convective range. Indeed, HBLRA predicts that the relaxation timescale of the scalar distribution within the viscous-convective range is dominated by a single timescale $\sim(\nu/\varepsilon)^{1/2}$ of the Kolmogorov scale, which is in accordance with the idea of Batchelor [10]. Our result of $C_B \approx 3.60$ is close to experimental values obtained from measurements of oceanic flows (3.9 ± 1.5 [11] and 3.7 ± 1.5 [12]). It should be remarked, however, that the pioneering works of Refs. [11,12] fully rely on the spectral form of Ref. [10], which has not been verified yet (a more recent work Ref. [15] reported that their DNS shows better agreement with another spectral form of Ref. [35] than that of Ref. [10]). Also, in the measurement of temperature field in oceanic flow, the Schmidt number ($\mathrm{Sc} \approx 10$) is not sufficiently high to obtain a clear k^{-1} spectrum, so their data alone may not be sufficient to verify our achievement (Refs. [11,12] determine C_B from the fitting of their measurements with the entire viscous range including the viscous-diffusive range). Another experiment on the mixing of salt concentration within water reported $C_B \approx 4$ from a clearer viscous-convective range [13]. Recent numerical surveys reported somewhat higher values of C_B: $C_B \approx 4.9$ from Ref. [14] by fitting their DNS data under moderate Schmidt numbers, $C_B \approx 5.7$ from Ref. [15] via high-Schmidt-number DNS with the Reynolds number being moderate, and $C_B \approx 5$ from Ref. [17] via high-Reynolds-number DNS with the Schmidt number being moderate. It may still be challenging with the current computational technology to increase both Reynolds and Schmidt numbers simultaneously, and thus our result $C_B \approx 3.60$ may be left as one theoretical prediction to be assessed by future studies.

Finite-Schmidt-number calculations suggest the existence of the universal viscous-convective range for high Sc ($\gtrsim$10 000). Our results indicate the existence of a buffer region $0.05 \lesssim k\eta \lesssim 1$ between the inertial-convective and the viscous-convective ranges, and the k^{-1} power-law range may appear in $k\eta \gtrsim 1$. Here we shall recall the assumption in deriving the spectrum of Eq. (4.15); our asymptotic analysis requires $k\eta \gg 1$, while our results of Figs. 7 and 8 appear to tend to the asymptotes for $k\eta \gtrsim 1$. Since both DNS and LRA suggest an appreciable falloff of the energy spectrum for $k\eta \gtrsim 0.1$ [25,36], it might be possible to relax the assumption from $k\eta \gg 1$ to $k\eta \gg 0.1$, which could partially support the existence of the viscous-convective range for $k\eta \gtrsim 1$. In the range $1 \lesssim k\eta \lesssim 30$ of the case $\mathrm{Sc} = 100\,000$, both the compensated spectrum and the timescale agree with the asymptotic values [$C_B \approx 3.60$ and $\tau_G \approx 2.53(\nu/\varepsilon)^{1/2}$] within the error of 3%, which could be recognized as the plateaus of the viscous-convective range (see Figs. 7 and 8).

On the other hand, the finite-Reynolds-number effect on the viscous-convective range should also be explored in future studies. One can make a rough projection of the finite-Reynolds-number effect using a discussion of Sec. V as follows. According to the function $\bar{F}$ in Fig. 5, the turbulence of a limited wave number band contributes to the scalar flux within the viscous-convective range. Indeed, the theory suggests that the velocity spectrum within a limited band $0.01 \leqslant k\eta \leqslant 1$ can express 99% of the scalar flux within the viscous-convective range. In DNS of the velocity field based on the pseudospectral method, for instance, if the energy pileup occurs around $k\eta \approx 1$ due to the wave number cutoff, this may contaminate the viscous-convective range via the scalar flux according to Eq. (4.18). If the schemes of forcing or time averaging affect the spectrum of $k\eta \approx 0.01$, the scalar flux may also be affected via Eq. (4.18). Then, in order to obtain the universal Batchelor constant with a certain accuracy, one may need to obtain, at least, the energy spectrum of $k\eta \lesssim 0.01$ with a sufficient accuracy.

There is still much room for improvement in the present framework, i.e., the incorporation of the intermittency effect. HBLRA, as a branch of the moment-closure theory, does not reflect the spatial

intermittency of ε and χ. However, the intermittency effect may be more prominent as the scale becomes small, and this should be taken into account. Up to now we have had no perspective on how much this affects our result: not only the predicted value of the Batchelor constant but even its universality may be questioned. Unfortunately, the problem is out of reach of the current work. However, low-Schmidt-number simulations confirmed stronger intermittency as the scale becomes small [7], and there should be an undeniable effect on the physics in the sub-Kolmogorov scale. In the same context, we mention the viscous-diffusive range ($k \gtrsim k_b$). For the high-wave number limit ($k \to \infty$), the asymptotic solution of Eqs. (3.1)–(3.3) yields $E_\theta(k) \propto \exp[-\sqrt{15}(k/k_b)^2]$ (algebraic dependence omitted), which shows a more rapid falloff than those expected from DNS [14,15]. This may be partially due to the lack of intermittency effect. Likewise in Ref. [15], incorporation of the spatial intermittency of the physical properties may be available to further investigate the physics of the far-dissipative range.

The present paper provides an application to the most fundamental case, i.e., fully developed homogeneous isotropic turbulence. There may be, however, further generalized cases to which the present formulation could contribute. For instance, turbulence induced by the Rayleigh-Taylor instability (RTI) may be one typical class of phenomena frequently observed in both industrial and natural sciences. Numerical and experimental studies on RTI-induced turbulence have examined a wide range of Sc (1–1000) [37], which could be compared with the result of Sec. V, where Sc ranges from 10 to 100 000. HBLRA may be a reasonable approach to phenomena of such a wide range of Sc. Also, we should note that as of now there is no conclusive argument about the inertial-range structure of RTI-induced turbulence [38,39]. In this respect, it should be recalled that LRA and HBLRA closures can be applied without assuming the velocity spectrum, so RTI should be an important subject for future studies. In particular, the constant-density formulation with the Boussinesq approximation may be available for current LRA and HBLRA formulations [40].

ACKNOWLEDGMENT

The author truly thanks the anonymous referees for their constructive comments, which have appreciably improved the quality of the present manuscript.

APPENDIX A: DERIVATION OF EQS. (3.1)–(3.3)

Here we begin with Eq. (2.3). First the integration domain $\triangle$ can be replaced with $\triangledown$. In $\triangledown$, q is close to k so that k, p, and q can form the sides of a triangle, i.e., $k, q \gg p$ and $q \approx k$. A simple replacement of q with k results in vanishing of the right side, and any nontrivial contributions may arise from a slight difference between k and q. Then we rewrite q as $k + \xi p$, where ξ ($\in [-1, 1]$) is a dimensionless parameter introduced to simplify the integration by q. Now Eq. (2.3) is rewritten as

$$(\partial_t + 2\kappa k^2)H(k;t,t) = 2\pi k \int_0^{p_{\max}} dp \int_{-1}^{1} (p\,d\xi)\, p(k+p\xi)(1-z^2) \int_{t_0}^{t} ds\, Q(p;t,s) \times \{H(k+p\xi;s,t)G_H(k;t,s) - H(k;s,t)G_H(k+p\xi;t,s)\}. \tag{A1}$$

Now we perform power series expansions in terms of $\hat{p}$ ($\equiv p/k$) as follows:

$$1 - z^2 = 1 - \xi^2 + \hat{p}\xi(1-\xi^2) + O(\hat{p}^2), \tag{A2}$$

$$H(k+p\xi;s,t) = H(k;s,t) + \hat{p}\xi\, k\frac{\partial H(k;s,t)}{\partial k} + \frac{1}{2}\hat{p}^2\xi^2\, k^2\frac{\partial^2 H(k;s,t)}{\partial k^2} + O(\hat{p}^3), \tag{A3}$$

$$G_H(k+p\xi;t,s) = G_H(k;t,s) + \hat{p}\xi\, k\frac{\partial G_H(k;t,s)}{\partial k} + O(\hat{p}^2). \tag{A4}$$

From the lowest order analysis in $\hat{p}$, Eq. (A1) turns into

$$(\partial_t + 2\kappa k^2)H(k;t,t) = \frac{4}{15}\pi^2 k^{-2}\int_0^{p_{\max}} dp \int_{t_0}^{t} ds\; p^4 Q(p;t,s) \times \left[G_H(k;t,s)\frac{\partial}{\partial k}\left\{k^4\frac{\partial H(k;s,t)}{\partial k}\right\} - H(k;s,t)\frac{\partial}{\partial k}\left\{k^4\frac{\partial G_H(k;t,s)}{\partial k}\right\}\right]. \tag{A5}$$

At this stage, we do not need to limit the p integration up to $p_{\max}$, since $Q(p;t,s)$ tends to zero for $p \geqslant p_{\max} \gg k_\eta$. Then we reach Eq. (3.1) free of the cutoff wave number $p_{\max}$. Similar steps can be applied to Eqs. (2.4) and (2.5), which results in Eqs. (3.2) and (3.3).

APPENDIX B: INTEGRATION OF $\bar{G}_H$

One simple approach to Eq. (4.3) may be an iteration scheme where one may repeatedly substitute an old $\bar{G}_H(\tau)$ into the right side and integrate the left to obtain a new $\bar{G}_H(\tau)$. It should be noted, however, that such a direct iteration does not converge well for large τ. An alternative approach may be given as follows. First we shall focus on the first term on the right side of Eq. (4.3):

$$-K(\tau)\bar{G}_H(\tau), \quad \left(K(\tau) \equiv \frac{4}{15}C_K\int_0^\infty d\bar{p}\;\bar{p}^{1/3}\int_0^\tau d\sigma\;\bar{Q}(\bar{p};\tau-\sigma)\right). \tag{B1}$$

This term implies that $\bar{G}_H(\tau)$ may decay exponentially as $\tau \to \infty$, which helps $\bar{G}_H(\tau)$ to converge at large τ. Let us extract the exponential behavior caused by this term by solving the following equation:

$$\partial_\tau \bar{A}(\tau) = -K(\tau)\bar{A}(\tau). \tag{B2}$$

Rewriting $\bar{A}(\tau)$ as $\exp[-\bar{a}(\tau)]$ and substituting it into Eq. (B2) yields

$$\partial_\tau \bar{a}(\tau) = K(\tau). \tag{B3}$$

Now we shall define the initial condition. Here we choose $\bar{a}(0) = 0$ for later simplicity. Also note that $\partial_\tau \bar{a}(\tau)|_{\tau=0}\; K(0) = 0$. Following a similar strategy to Ref. [28], we differentiate both sides by τ, which reads

$$\partial_\tau^2 \bar{a}(\tau) = \frac{4}{15}C_K\int_0^\infty d\bar{p}\;\bar{p}^{1/3}\bar{Q}(\bar{p};\tau). \tag{B4}$$

Now Eq. (B4) can be solved with the help of its initial conditions: $\bar{a}(0) = 0$ and $\partial_\tau \bar{a}(\tau)|_{\tau=0} = 0$.

Let us next express $\bar{G}_H(\tau)$ using the above exponential decay factor. Introducing another dimensionless function $\bar{B}(\tau)$, we write $\bar{G}_H(\tau)$ as $\bar{A}(\tau)\bar{B}(\tau)$. Substituting this into Eq. (4.3) yields

$$\partial_\tau \bar{B}(\tau) = \frac{1}{\bar{A}(\tau)}\frac{4}{15}C_K\int_0^\infty d\bar{p}\;\bar{p}^{1/3}\int_0^\tau d\sigma\;\bar{Q}(\bar{p};\tau-\sigma)\bar{G}_H(\tau-\sigma)\bar{G}_H(\sigma), \tag{B5}$$

accompanied by $\bar{G}_H(\tau) = \bar{A}(\tau)\bar{B}(\tau)$. The initial condition $\bar{G}_H(0) = 1$ is now expressed by $\bar{B}(0) = 1$. One can apply the iteration scheme to $\bar{B}(\tau)$, which shows much faster and stabler convergence than that of the iteration based on $\bar{G}_H(\tau)$. Starting from the initial function $\bar{B}(\tau) = 1$, ten iterations may be sufficient to obtain $\tau_G \approx 2.53$. The numerical solutions for $\bar{G}_H(\tau)$, $\bar{A}(\tau)$, and $\bar{B}(\tau)$ are shown in Fig. 9. While $\bar{B}(\tau)$ oscillates for a wide range of τ, the exponential decay of $\bar{A}(\tau)$ rapidly damps $\bar{G}_H(\tau)$. Similar steps may be applicable to $\bar{R}(\tau)$.

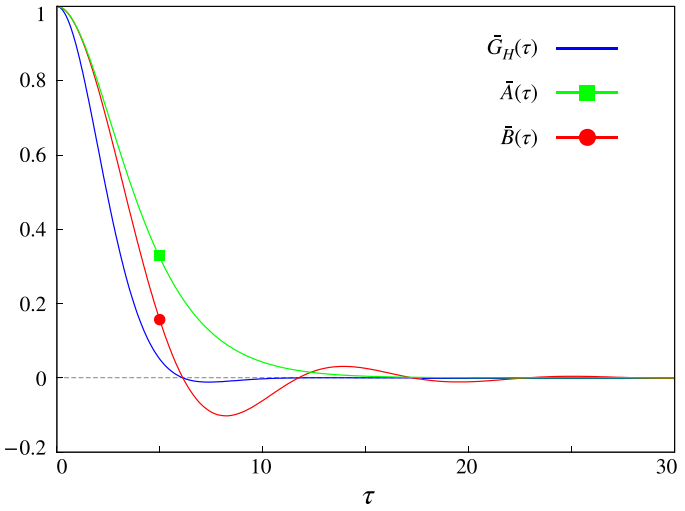

FIG. 9. Profiles of $\bar{G}_H(\tau)$, $\bar{A}(\tau)$, and $\bar{B}(\tau)$.

APPENDIX C: DERIVATION OF EQ. (4.15)

Using dimensionless functions ($\bar{Q}$, $\bar{R}_H$, and $\bar{G}_H$) and the scalar-variance spectrum $E_\theta(k)$ [$= 4\pi k^2 H(k)$], Eq. (4.14) may be rewritten as

$$\Pi_\theta(k) = -\frac{2}{15} C_K \left(\frac{\varepsilon}{\nu}\right)^{1/2} k^3 \frac{\partial\, k^{-1} E_\theta(k)}{\partial k} \int_0^\infty d\bar{p}\, \bar{p}^{1/3} \int_0^\infty d\sigma\, \bar{Q}(\bar{p},\sigma)\bar{R}_H(-\sigma)\bar{G}_H(\sigma). \tag{C1}$$

The above $\Pi_\theta(k)$ should be balanced with χ: $\Pi_\theta(k) = \chi$ [see Eq. (4.12)], which may be rewritten as

$$k^3 \frac{\partial\, k^{-1} E_\theta(k)}{\partial k} = -\frac{15}{2C_K} \chi \left(\frac{\nu}{\varepsilon}\right)^{1/2} \Bigg/ \int_0^\infty d\bar{p}\, \bar{p}^{1/3} \int_0^\infty d\sigma\, \bar{Q}(\bar{p},\sigma)\bar{R}_H(-\sigma)\bar{G}_H(\sigma). \tag{C2}$$

Now Eq. (C2) may be regarded as a first-order differential equation of $E_\theta(k)$, which can be integrated in a straightforward manner:

$$E_\theta(k) = C_B \chi \left(\frac{\nu}{\varepsilon}\right)^{1/2} k^{-1} + Ck, \tag{C3}$$

with

$$C_B = \frac{5}{2C_K} \Bigg/ \int_0^\infty d\bar{p}\, \bar{p}^{1/3} \int_0^\infty d\sigma\, \bar{Q}(\bar{p},\sigma)\bar{R}_H(-\sigma)\bar{G}_H(\sigma). \tag{C4}$$

Here C is an arbitrary constant, which should vanish for a physically acceptable solution convergent for $k \to \infty$. Then we reach Eq. (4.15).

[1] A. M. Obukhov, Structure of the temperature field in turbulent flow, Izv. Akad. Nauk SSSR Geophr. Geofiz. **13**, 58 (1949) [translated by Foreign Technology Division, Air Force System Command, USA (1970)].

[2] S. Corrsin, On the spectrum of isotropic temperature fluctuations in an isotropic turbulence, J. Appl. Phys. **22**, 469 (1951).

[3] K. R. Sreenivasan, The passive scalar spectrum and the Obukhov-Corrsin constant, Phys. Fluids **8**, 189 (1996).
[4] L. Mydlarski and Z. Warhaft, Passive scalar statistics in high-Péclet-number grid turbulence, J. Fluid Mech. **358**, 135 (1998).
[5] L. P. Wang, S. Chen, and J. G. Brasseur, Examination of hypotheses in the Kolmogorov refined turbulence theory through high-resolution simulations. Part 2. Passive scalar field, J. Fluid Mech. **400**, 163 (1999).
[6] P. K. Yeung, S. Xu, and K. R. Sreenivasan, Schmidt number effects on turbulent transport with uniform mean scalar gradient, Phys. Fluids **14**, 4178 (2002).
[7] T. Watanabe and T. Gotoh, Statistics of a passive scalar in homogeneous turbulence, New J. Phys. **6**, 40 (2004).
[8] P. K. Yeung, D. A. Donzis, and K. R. Sreenivasan, High-Reynolds-number simulation of turbulence mixing, Phys. Fluids **17**, 081703 (2005).
[9] T. Gotoh and T. Watanabe, Power and nonpower laws of passive scalar moments convected by isotropic turbulence, Phys. Rev. Lett. **115**, 114502 (2015).
[10] G. K. Batchelor, Small-scale variation of convected quantities like temperature in turbulent fluid. Part 1. General discussion and the case of small conductivity, J. Fluid Mech. **5**, 113 (1959).
[11] H. L. Grant, B. A. Hughes, R. B. Williams, and A. Moillient, The spectrum of temperature fluctuations in turbulent flow, J. Fluid Mech. **34**, 423 (1968).
[12] N. S. Oakey, Determination of the rate of dissipation of turbulent energy from simultaneous temperature and velocity shear microstructure measurements, J. Phys. Oceanogr. **12**, 256 (1982).
[13] C. H. Gibson and W. H. Schwarz, The universal equilibrium spectra of turbulent velocity and scalar fields, J. Fluid Mech. **16**, 365 (1963).
[14] D. A. Donzis, K. R. Sreenivasan, and P. K. Yeung, The Batchelor spectrum for mixing of passive scalars in isotropic turbulence, Flow, Turbul. Combust. **85**, 549 (2010).
[15] T. Gotoh, T. Watanabe, and H. Miura, Spectrum of passive scalar at very high Schmidt number in turbulence, Plasma Fusion Res. **9**, 3401019 (2015)
[16] D. Buaria, M. P. Clay, K. R. Sreenivasan, and P. K. Yeung, Turbulence is an ineffective mixer when Schmidt numbers are large, Phys. Rev. Lett. **126**, 074501 (2021).
[17] K. P. Shete, D. J. Boucher, J. J. Riley, and S. M. de Bruyn Kops, Effect of viscous-convective subrange on passive scalar statistics at high Reynolds number, Phys. Rev. Fluids **7**, 024601 (2022).
[18] C. H. Gibson, Fine structure of scalar fields mixed by turbulence. II. Spectral theory, Phys. Fluids **11**, 2316 (1968).
[19] J. Qian, The spectrum of a turbulent passive scalar in the viscous-convective range, J. Fluid Mech. **217**, 203 (1990).
[20] R. H. Kraichnan, The structure of isotropic turbulence at very high Reynolds numbers, J. Fluid Mech. **5**, 497 (1959).
[21] R. H. Kraichnan, Lagrangian-history closure approximation for turbulence, Phys. Fluids **8**, 575 (1965).
[22] R. H. Kraichnan and J. R. Herring, A strain-based Lagrangian-history turbulence theory, J. Fluid Mech. **88**, 355 (1978).
[23] R. H. Kraichnan, Eulerian and Lagrangian renormalization in turbulence theory, J. Fluid Mech. **83**, 349 (1977).
[24] Y. Kaneda, Renormalized expansions in the theory of turbulence with the use of the Lagrangian position function, J. Fluid Mech. **107**, 131 (1981).
[25] S. Kida and S. Goto, A Lagrangian direct-interaction approximation for homogeneous isotropic turbulence, J. Fluid Mech. **345**, 307 (1997).
[26] R. H. Kraichnan, Dispersion of particle pairs in homogeneous turbulence, Phys. Fluids **9**, 1937 (1966).
[27] J. R. Herring and R. H. Kraichnan, A numerical comparison of velocity-based and strain-based Lagrangian-history turbulence approximation, J. Fluid Mech. **91**, 581 (1979).
[28] Y. Kaneda, Inertial range structure of turbulent velocity and scalar fields in Lagrangian renormalized approximation, Phys. Fluids **29**, 701 (1986).
[29] S. Goto and S. Kida, Passive scalar spectrum in isotropic turbulence: Prediction by the Lagrangian direct-interaction approximation, Phys. Fluids **11**, 1936 (1999).

[30] Y. Kaneda, Lagrangian renormalized approximation of turbulence, Fluid Dyn. Res. **39**, 526 (2007).
[31] T. Ariki and K. Yoshida, Hessian-based Lagrangian closure theory for passive scalar turbulence, Phys. Rev. Fluids **6**, 104603 (2021).
[32] T. Ariki, K. Yoshida, K. Matsuda, and K. Yoshimatsu, Scale-similar clustering of heavy particles in the inertial range of turbulence, Phys. Rev. E **97**, 033109 (2018).
[33] Y. Zhou, Turbulence theories and statistical closure approaches, Phys. Rep. **935**, 1 (2021).
[34] T. Gotoh, Passive scalar diffusion in two-dimensional turbulence in the Lagrangian renormalized approximation, J. Phys. Soc. Jpn. **58**, 2365 (1989).
[35] R. C. Mjolsness, Diffusion of passive scalar at large Prandtl number according to abridged Lagrangian interaction theory, Phys. Fluids **18**, 1393 (1975).
[36] T. Ishihara, K. Morishita, M. Yokokawa, A. Uno, and Y. Kaneda, Energy spectrum in high-resolution direct numerical simulations of turbulence, Phys. Rev. Fluids **1**, 082403(R) (2016).
[37] Y. Zhou, Rayleigh–Taylor and Richtmyer–Meshkov instability induced flow, turbulence, and mixing. II, Phys. Rep. **723**, 1 (2017).
[38] Y. Zhou, A scaling analysis of turbulent flows driven by Rayleigh–Taylor and Richtmyer–Meshkov instabilities, Phys. Fluids **13**, 538 (2001).
[39] A. W. Cook and Y. Zhou, Energy transfer in Rayleigh-Taylor instability, Phys. Rev. E **66**, 026312 (2002).
[40] Y. Zhou, R. J. R. Williams, P. Ramaprabhu, M. Groom, B. Thornber, A. Hillier, W. Mostert, B. Rollin, S. Balachandar, P. D. Powell, A. Mahalov, and N. Attal, Rayleigh–Taylor and Richtmyer–Meshkov instabilities: A journey through scales, Physica D **423**, 132838 (2021).